Experimental Cell Research 438 (2024) 114061

Contents lists available at ScienceDirect

Experimental Cell Research

journal homepage: www.elsevier.com/locate/yexcr

Research article

Pyroptosis inhibitors MCC950 and VX-765 mitigate myocardial injury by alleviating oxidative stress, inflammation, and apoptosis in acute myocardial hypoxia

Xing Ye [a,b], Zi-jie Lin [a], Guang-hui Hong [a], Zhi-min Wang [a], Run-ting Dou [a], Jun-yi Lin [a], Jian-hui Xie [a], Yi-wen Shen [a,*]

[a] Department of Forensic Medicine, School of Basic Medical Sciences, Fudan University, Shanghai, 200032, China
[b] Department of Forensic Medicine, School of Basic Medical Sciences, Gannan Medical University, Ganzhou, 341000, China

ARTICLE INFO

Keywords:
Acute myocardial infarction
Hypoxia
Pyroptosis
NLRP3 inflammasome

ABSTRACT

Acute myocardial infarction (AMI) is a prevalent cardiovascular disease with high morbidity and mortality rates worldwide. Pyroptosis is an inflammatory form of programmed cell death that has been linked to various pathological conditions. However, its exact contribution to the onset and progression of heart injury in AMI has not yet fully elucidated. Herein, we established mouse AMI model by ligating the left anterior descending artery and performed transcriptome analysis during the early phase of AMI. Mouse HL-1 and human AC-16 cardiomyocytes were subjected to hypoxia to simulate ischemic injury in vitro. Our results revealed a significant activation of the inflammatory response at 3 h post-ligation, as confirmed by RNA sequencing. We identified the occurrence of NLRP3 inflammasome-mediated pyroptosis in the cardiac tissues of human cases with AMI, as well as in mouse models of AMI and hypoxia-induced cardiomyocytes, using immunohistochemistry staining and Western blotting assays. Concurrently, pharmacological inhibition of NLRP3 inflammasome-mediated pyroptosis with MCC950 and VX-765 effectively decreased hypoxia-induced cardiomyocytes injury, while mitigating myocardial oxidative stress, apoptosis and inflammation caused by hypoxia. Moreover, the circulating levels of gasdermin D (GSDMD), the pyroptosis executor, were remarkably elevated in the plasma of mice with early AMI and in the supernatant of hypoxia-exposed cardiomyocytes in a time-dependent manner using ELISA and Western blotting. Furthermore, the change in circulating GSDMD positively correlated with Creatine Kinase-MB (CK-MB) in the plasma of early-stage AMI mouse. In summary, these findings indicated a critical role for NLRP3 inflammasome-mediated pyroptosis in the progression of AMI, the administration of MCC950 and VX-765 may be attractive candidate therapeutic approaches for cardiac injury caused by acute hypoxia or even AMI. Additionally, the circulating GSDMD exhibits potential as a newly diagnostic biomarker for AMI.

1. Introduction

Acute myocardial infarction (AMI) is typically triggered by sudden coronary artery occlusion resulting in ischemic necrosis of the corresponding myocardium due to insufficient blood supply [1]. Prolonged myocardial ischemia can lead to structural and functional abnormalities in heart, which can progress to heart failure and ultimately culminate in sudden cardiac death [2,3]. While advancements in treatment methods such as venous thrombolysis and percutaneous coronary intervention have significantly reduced the mortality rate of AMI, there has been a noticeable increase in the risk of post-MI heart failure [4]. Timely and effective diagnosis and treatment of AMI patients can significantly improve therapeutic outcomes and enhance patient survival rates. In clinical practice, CK-MB and cardiac troponins are widely utilized as valuable indictors for diagnosing AMI [5,6], but they are challenged by lack of specificity [7,8]. Therefore, further exploration of drugs that can shield against AMI-induced myocardial injury holds significant promise. Additionally, the search for novel and specific early diagnostic biomarkers for AMI can guide precise diagnosis of the condition.

The development of AMI is widely recognized to involve oxidative stress, inflammation, and subsequent cardiomyocyte apoptosis. During AMI, a robust inflammatory process is essential for effective myocardial

* Corresponding author.
E-mail address: shenyiwen@fudan.edu.cn (Y.-w. Shen).

https://doi.org/10.1016/j.yexcr.2024.114061
Received 19 December 2023; Received in revised form 26 April 2024; Accepted 28 April 2024
Available online 30 April 2024

injury healing. However, it can also give rise to an overabundance of damage and disruption in ventricular remodeling, eventually leading to the manifestation of heart failure and compromised myocardial function [9]. Research indicates that the nuclear factor-κB signaling pathway plays a pivotal role in the inflammatory injury of AMI, with its activation triggering the production of various proinflammatory cytokines, including tumor necrosis factor-alpha (TNF-α), interleukin-1 beta (IL-1β), and IL-6 [10]. Leukocytes are drawn into the injured myocardium following the release of multiple inflammatory factors, which further worsens oxidative stress and inflammatory damage.

Emerging evidence suggests that the pathophysiological process of myocardial ischemia or death in AMI is significantly influenced by oxidative stress, induced by an excess of reactive oxygen species (ROS) [11]. The overproduction of ROS disrupts the redox state balance and triggers cell apoptosis, ultimately exacerbating myocardial injury and worsening cardiac function [12]. It is important to highlight that oxidative stress also directly promotes the expression of inflammatory cytokines and inducing leukocyte chemotaxis, thus intensitying the inflammatory process [13]. In addition, oxidative stress is the primary factor contributing to the unfavorable prognosis associated with myocardial damage induced by AMI [14]. Apoptosis is also a key pathologic feature of AMI and contributes to cardiomyocyte cell injury [15]. Further, apoptosis is considered the primary cause responsible for myocardial cell loss following AMI, and it is strongly linked to ventricular remodeling and the subsequent development of heart failure [16,17]. Therefore, these studies lay a foundation for therapeutically targeting inflammation, oxidative stress and apoptosis as an effective strategy to mitigate AMI-induced cardiac injury.

Myocardial injury resulting from AMI is predominantly attributed to the demise of terminally differentiated cardiomyocytes [17]. Pyroptosis is a newly recognized inflammatory form of programmed cell death that commonly occurs in the presence of inflammatory conditions [18]. The hallmark features of pyroptosis comprise the activation of inflammasome, the cleavage of gasdermin-D (GSDMD), and the subsequent formation of membrane pores [19,20]. Nucleotide-binding oligomerization domain-like receptor pyrin domain-containing 3 (NLRP3) inflammasome initiates self-cleavage of pro-caspase1, and activated caspase1 cleaves GSDMD to generate the N-terminal fragments of GSDMD (GSDMD-NT) that trigged membrane pore formation, eventually leads to the unleashing of inflammatory factors, loss of membrane integrity, and pyroptosis [21,22]. Pyroptosis, as an essential component of the body's innate immune defense system, assumes a pivotal function in safeguarding against infectious agents [23]. However, excessive pyroptosis have detrimental effects on the host [24]. Numerous studies have demonstrated that pyroptosis is an irreplaceable signaling cascade contributing to myocardial cell death [25,26]. Nonetheless, the functions of cardiomyocytes pyroptosis, its potential relationship with AMI, and the underlying molecular mechanisms remain largely elusive.

This study sought to investigate the influence of pyroptosis on myocardial injury following hypoxia and evaluate whether the implicated mechanisms are associated with alternations in myocardial inflammation, oxidative stress and apoptosis induced by acute myocardial hypoxia. Additionally, given the release of GSDMD from pyroptotic cardiomyocytes [27], we hypothesized that it holds promise as a potential diagnostic biomarker for AMI.

2. Materials and methods

2.1. Antibodies and reagents

Antibodies against TMS1/ASC (DF6304), Cleaved Caspase-1 (AF4022), and GSDMD (AF4012) were obtained from Affinity Bioscience (Cincinnati, OH, United States). The anti-β-actin (66009-1-Ig), anti-p67phox (15551-1-AP), and anti-BAX (60267-1-Ig) were provided by ProteinTech Group. NLRP3 (15101), Cleaved Caspase3 (9661), TNF-α (11948) were bought from Cell Signaling Technology (Beverly, Massachusetts, United States). Phosphor–NF–κB p65 (TP56371), NF-κB p65 (T55034), IL-6 (TD6087) were obtained from Abamrt (Shanghai, China). MMP9 (A0289) was purchased from Abclonal (Boston, MA, USA). BCL-2 (ab194583) was bought from Abcam (Cambridge, UK). Anti-NLRP3 for immunohistochemistry staining (NBP2-12446, 1:50) was purchased from Novus Biologicals (Minnesota, United States). MCC950 (HY-12815) and VX-765 (HY-13205) were bought from MedChemExpress (Shanghai, China).

2.2. Human subjects

The human heart samples were obtained from autopsy cases conducted by the Department of Forensic Medicine at School of Basic Medical Sciences, Fudan University (Shanghai, China). The cases were categorized into two distinct groups: the control group (n = 3) and AMI group (n = 3). The control group comprised individuals who suffered acute traumatic death due to cranial injuries from traffic accidents, with no apparent gross or microscopic cardiac pathological findings. The inclusion criteria for the AMI group were based on histological observations indicating early myocardial ischemia, such as hyper eosinophilia of cardiomyocytes, wavy fibers, interstitial edema, and contraction band necrosis, along with coronary atherosclerosis of more than 50 %, while excluding obvious gross cardiac pathology or other non-cardiac causes. The cause of death for these groups was diagnosed by at least two forensic pathologists. The Supplementary Table 1 presents detailed characteristics of both study groups. Our study was granted by the Medical Ethics Committee of School of Basic Medical Sciences, Fudan University (approval no.: 2023-030).

2.3. Establishment of AMI mouse model

Male C57BL/6 mice, aged between 6 and 8 weeks, were utilized in this study. The mouse AMI model was constructed by ligating the left anterior descending coronary artery (LAD) following the previously described [28]. Briefly, mice were anesthetized with 2 % isoflurane and intubated for ventilation. The chest cavity was carefully opened to expose the hearts, and a 7-0 silk suture was skillfully employed to ligate the LAD. The presence of ischemia was visually confirmed by observing a pale color in the myocardium, and its assessment was conducted utilizing a II lead electrocardiogram. After the surgical procedure, mice were euthanized at time points of 1 h, 3 h, and 6 h after the onset of myocardial ischemia (n = 10 each group). The sham group (n = 10) underwent identical processes without the ligation step. Plasma samples were prepared from all mice by collecting orbital vein blood. All animal experiments were conducted with the approval of the Experimental Animal Ethics Committee of School of Basic Medical Sciences, Fudan University (approval no.:20231017-002).

2.4. Echocardiography

To evaluate cardiac function following AMI, mice were administered 2 % isoflurane anesthesia and subsequently underwent echocardiography. The left ventricular end-systolic diameter (LVESd) and left ventricular end-diastolic diameter (LVEDd) were measured using long-axis M-mode. The ejection fraction (EF) was utilized to assess the cardiac contractile function.

2.5. Histological analysis and immunohistochemistry (IHC) staining

After the immediate sacrifice of mice, heart samples were soaked in a 4 % buffered formalin for 24 h. Subsequently, the specimens were carefully embedded in paraffin and meticulously sectioned into 4 μm thick slices. Hematoxylin & Eosin (H&E) staining was conducted for the histological examination of cardiac tissue using light microscopy.

IHC staining was conducted according to our previously published method [29]. Briefly, heart sections were deparaffinized and hydrated

before treatment with 3 % H_2O_2 to quench endogenous peroxidase activity. The specimens underwent a blocking step using goat serum for 30 min at room temperature. After that, the heart tissues were exposed to pyroptosis-related primary antibodies overnight at 4 °C and subsequently incubated with secondary antibodies for 60 min at 37 °C. Ultimately, the slides were visualized by diaminobenzidine (DAB) staining.

2.6. Cell culture and treatment

Human AC-16 and mouse HL-1 cardiomyocytes were cultured in DMEM enriched with 10 % fetal bovine serum at 37 °C in 5 % CO_2. To simulate an in vitro ischemic model, we referred to previous method [30,31]. In brief, HL-1 and AC-16 cardiomyocytes were subjected to a hypoxic environment of 1 % O_2 for 1 h, 3 h, and 6 h in serum-free medium. To inhibit NLRP3 inflammasome-mediated pyroptosis, specific small molecule inhibitors MCC950 (10 μM) and VX-765 (2 μM) [32] were pre-treated for 3 h before the hypoxia treatment in cardiomyocytes.

2.7. Cell counting kit-8 (CCK-8) assay

HL-1 and AC-16 cells were plated in 96-well plates and exposed to hypoxia treatment with or without MCC950 or VX-765. Subsequently, the cells' vitality was assessed using the CCK-8 assay in accordance with CCK-8 kit's manufacturer's instructions (A311-02, Vazyme Biotech). A microplate reader was employed to calculate the absorbance or optical density at 450 nm.

2.8. Calcein/PI fluorescent staining

Cell viability or pyroptosis was detected using Calcein/PI (Beyotime, Shanghai, China) staining. Briefly, cardiac HL-1 cells were cultured in 24-well plates and then exposed to 6 h of hypoxia treatment with or without MCC950 or VX-765. Subsequently, the cells were incubated with Calcein/PI and observed under a fluorescence microscopy.

2.9. Western blotting

Proteins from myocardial tissue and cardiomyocyte were isolated using RIPA buffer (Beyotime, Shanghai, China) containing protease and phosphatase inhibitors. Protein extraction from AC16 cell supernatant was adapted from a previous publication [33]. Briefly, cell supernatant was collected and centrifuged to eliminate cell debris and other impurities, followed by precipitation or concentration using methanol and chloroform. The protein concentrations were quantified using a BCA protein assay kit (Beyotime, Shanghai, China). Subsequently, the protein samples underwent 12 % sodium dodecyl sulfate polyacrylamide gel electrophoresis and were then transferred onto a polyvinylidene difluoride (PVDF) membrane. Following the blocking step using 5 % BSA at 37 °C for 1 h, the PVDF membranes were treated with specific primary antibodies targeting the proteins of interest overnight at 4 °C. These membranes were then exposed to the appropriate secondary antibodies for 1 h at room temperature, followed by detection using an enhanced chemiluminescence (ECL) kit from Thermo Scientific Fisher. β-actin was employed as the internal reference. The gel images were captured and subjected to analysis using Image-J software.

2.10. Enzyme-linked immunosorbent assay (ELISA)

After collecting plasma samples from mice or cell supernatants from cell culture, the levels of circulating GSDMD and CK-MB were measured using GSDMD ELISA kit (ab233627, Abcam) and CK-MB ELISA kit (EM30650, Biotech Well, Shanghai, China), respectively, following the manufacturer's instructions.

2.11. Measurement of ROS and oxidative stress

For measurement of intracellular ROS level, cardiac HL-1 cells were incubated at 37 °C for 30 min after being exposed to 10 μM DCFH-DA (Beyotime, Shanghai, China). The ROS was observed by a fluorescence microscope.

2.12. TdT-mediated dUTP nick end labeling (Tunel) staining

HL-1 cells were cultured in 24-well plates and fixed with 4 % polyformaldehyde. Subsequently, Tunel staining was performed to assess cardiac cell apoptosis following the manufacturer's protocol. The kit (A111-02, Vazyme Biotech) was labeled with FITC fluorescein, leading to green staining of apoptotic cells. Cell nuclei were stained using DAPI, followed by observation under a fluorescence microscope.

2.13. RNA sequence (RNA-seq) analysis

For RNA-seq, Trizol reagent was employed for the isolation of total RNA from both AMI-3h ($n = 3$) and sham ($n = 3$) heart tissues. The quality of RNA samples was assessed before constructing cDNA libraries, which were then sequenced by Majorbio Biotech (Shanghai, China). The differentially expressed genes (DEGs) between the AMI-3h group and the sham group were identified using criteria of $|\log2 \text{ Fold Change (FC)}| > 2$ and q value < 0.05. Furthermore, function enrichment analysis such as Gene Ontology (GO) and Kyoto Encyclopedia of Genes and Genomes (KEGG) was conducted. Significant enrichment was determined by adjusted p value < 0.05.

2.14. Statistical analysis

The data were displayed as mean ± standard error of the mean (SEM). Graphical representation and statistical analysis were conducted using GraphPad Prism 8.0 (GraphPad Software, Inc.). For comparisons among different groups, a one-way analysis of variance (ANOVA) or two-way ANOVA was employed followed by Turkey or Bonferroni's multiple comparison test where appropriate. Differences between the two groups were assessed using an unpaired Student's t-test. Statistical significance was defined as $p < 0.05$.

3. Results

3.1. Establishment and transcriptome profiling of mouse AMI model

Initially, we constructed the AMI mouse model varying ischemia durations (1 h, 3 h, and 6 h) by ligating LAD. Electrocardiogram (ECG) monitoring revealed a significant elevation of the ST segment by 3 h post-AMI (AMI-3h), while the ST segment remained at the baseline level in the sham group (Fig. 1A). Echocardiography results demonstrated a notable reduction in left ventricular ejection fraction (EF) in the AMI-3h group compared to the sham group (Fig. 1B), conforming to the manifestation of AMI. H&E staining (Fig. 1C) was conducted to assess the histological changes in the heart tissues of both the AMI and sham groups. The myocardium in the sham group exhibited normal cardiomyocyte morphology, whereas the AMI group displayed localized interstitial edema (black arrow) and wavy fibers (white arrow) with increased eosinophilia of the cytoplasm (green arrow).

To depict the molecular changes and biological processes involved in the early stages of AMI, RNA-seq analysis was conducted on the infarcted myocardial tissues from the AMI-3h and sham groups. A total of 254 differentially expressed genes (DEGs) were identified in the AMI-3h group compared to the sham group ($|\log2FC| > 2$ and adjusted p value < 0.05), with 226 genes showing up-regulation and 28 genes displaying down-regulation (Fig. 1D). Subsequently, GO and KEGG enrichment analyses were used to gain a deeper understanding of DEGs' biological function. GO analysis indicated a noteworthy abundance of

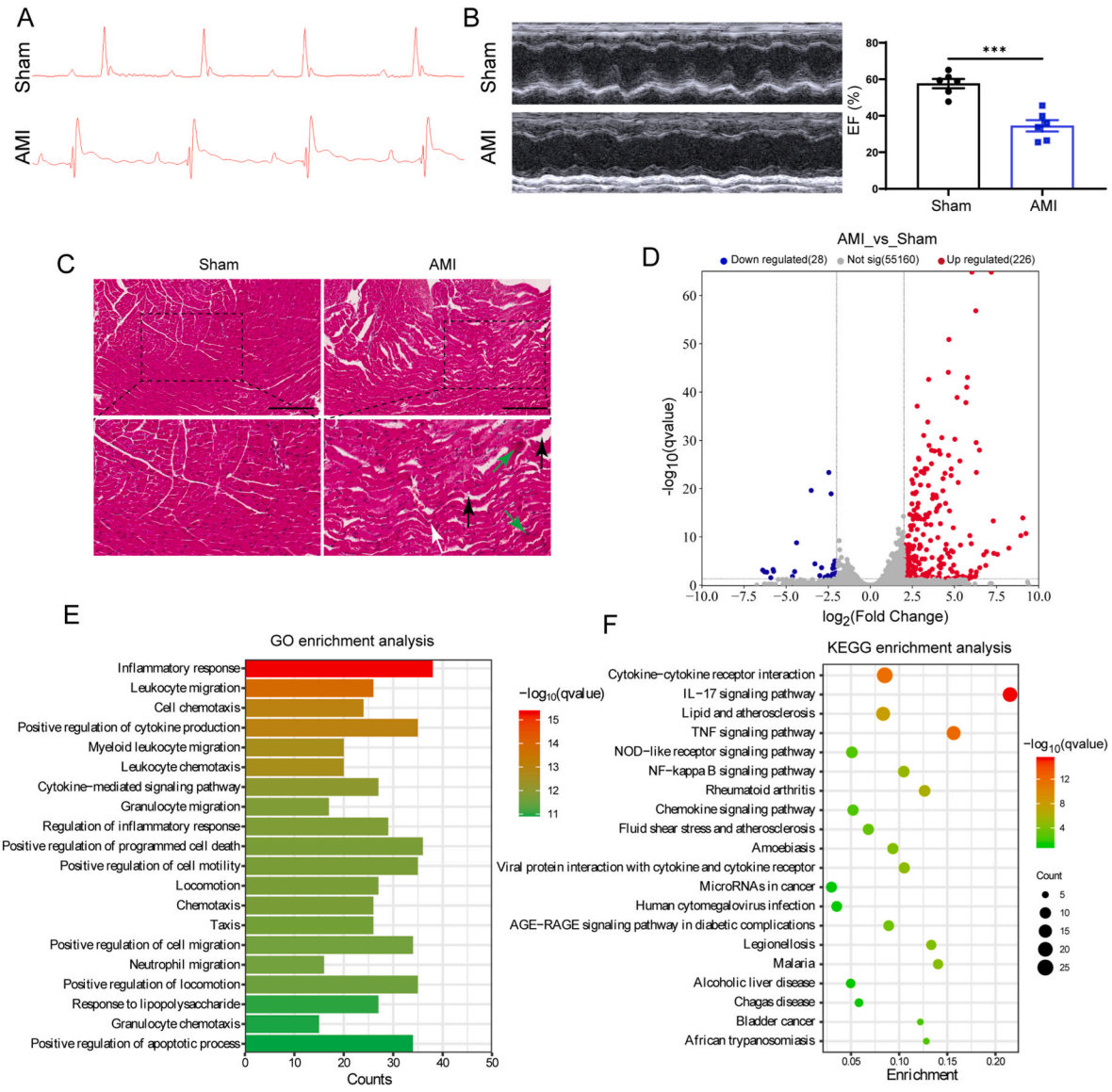

Fig. 1. Establishment of mouse AMI model and transcriptome analysis. (A) ECG monitoring in mice 3 h after AMI (AMI-3h) and sham groups. (B) Representative echocardiograms of AMI-3h and sham groups showed a decrease in cardiac contractile function in mice following AMI (n = 6, ***p < 0.001). (C) The representative Hematoxylin & Eosin (H&E) staining images of heart tissues for each group. Black arrow indicated interstitial edema, white arrow indicated wavy fibers and green arrow indicated hypereosinophilia of some cardiomyocytes. Scale bar = 200 μm. (D) Volcano map showing DEGs (|log2FC|> 2 and adjusted p value < 0.05) in the AMI-3h vs sham group (n = 3). (E) Bar chart depicting the significantly enriched GO classification of DEGs in term of biological process. (F) Bubble diagram shows KEGG pathway enrichment analysis of DEGs.

DEGs in pathways associated with inflammatory responses, including leukocyte migration, leukocyte chemotaxis (Fig. 1E). Additionally, the regulation of programmed cell death or apoptotic process was significantly activated. Consistently, KEGG pathway analysis revealed that the most significant functional pathways were related to cytokine−cytokine receptor interaction, NOD−like receptor signaling pathway, TNF signaling pathway, IL-17 signaling pathway, NF−kappa B signaling pathway, and chemokine signaling pathway (Fig. 1F), which were closely associated with inflammation and immune process. These findings suggest that the inflammatory system is activated during the early phase of AMI.

3.2. NLRP3 inflammasome and pyroptosis are activated by AMI

Pyroptosis is a form of inflammation-dependent programmed cell death mediated by inflammasomes [23,34]. The NLRP3 inflammasome sensor is widely characterized in the heart and is of utmost importance in the pathogenesis of various cardiovascular diseases [35,36]. Given the significant activation of inflammatory responses and programmed cell death processes during early AMI as indicated by our transcriptome analysis, we investigated whether NLRP3 inflammasome-mediated pyroptosis occurs in AMI. To address this, NLRP3-mediated pyroptosis-related proteins, including GSDMD, Caspase-1, ASC, and NLRP3 were assessed by Western blotting and immunohistochemical staining in human heart samples from individuals with AMI, as well as in *in vivo* and in vitro experiments.

Initially, heart specimens were collected from authentic autopsy cases of individuals who died from AMI and non-AMI (control group). The basic information of the deceased in the autopsy cases is presented in Supplementary Table 1. Immunohistochemistry assays revealed intense staining of ASC, cleaved caspase-1, and NLRP3 in the hearts of AMI compared to the control group (Fig. 2A). Furthermore, we found that the expression level of ASC, cleaved caspase-1, NLRP3, and GSDMD-NT gradually increased with the extension of myocardial ischemia

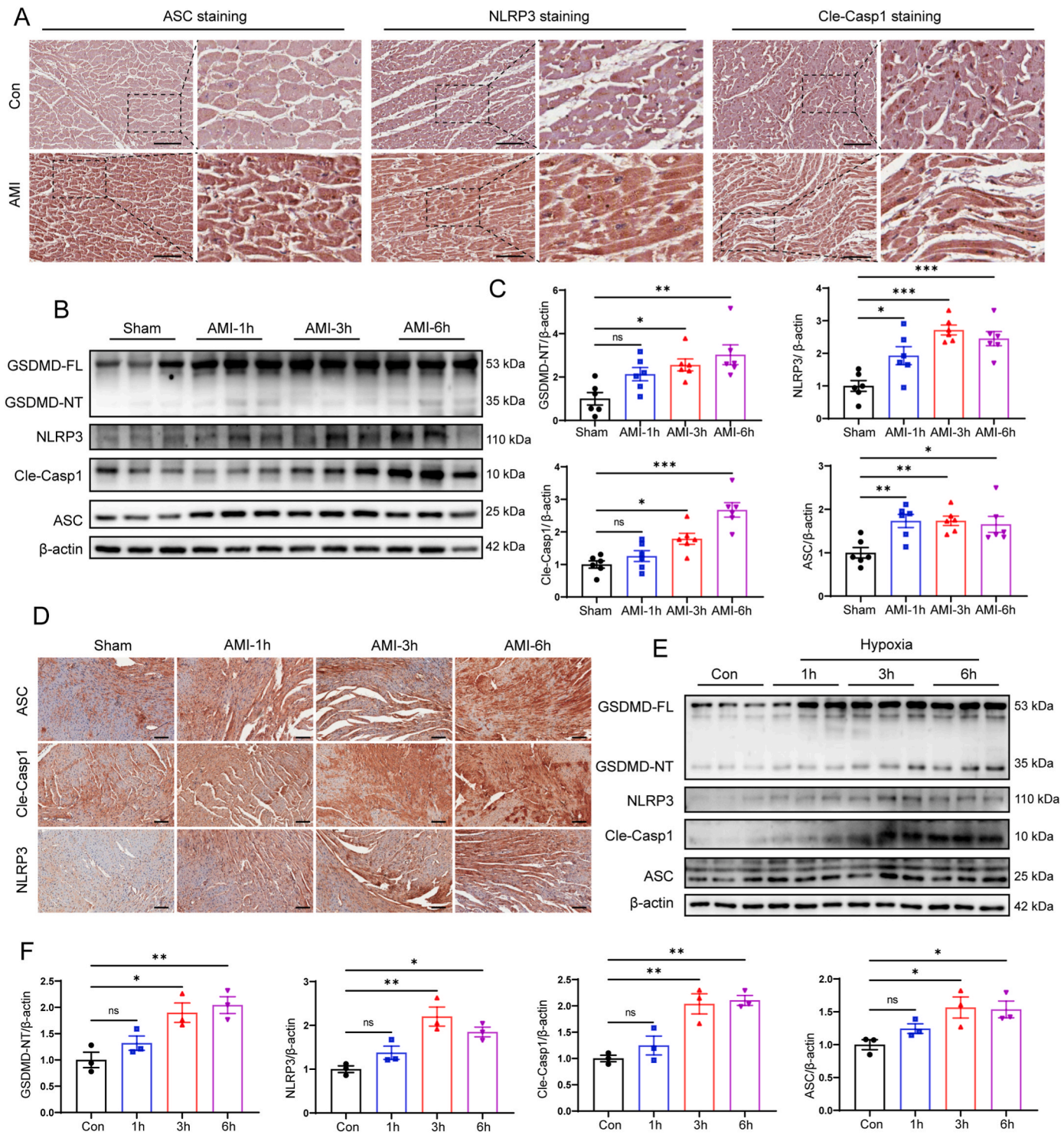

Fig. 2. The activation of NLRP3 inflammasome and pyroptosis during the early stages of AMI. (A) The representative immunohistochemistry staining images of ASC, NLRP3, and cleaved Caspase1 (Cle-Casp1) within the human heart sections. Scale bar = 100 μm. (B) The representative Western blotting bands of NLRP3 inflammasome and pyroptosis-associated proteins (ASC, NLRP3, Cle-Caps1, and GSDMD-NT) at different time points in AMI, n = 6 per group. (C) Quantification of the results of B, n = 6 per group. (D) The representative immunohistochemistry staining images of ASC, NLRP3, and Cle-Casp1 within the mouse AMI heart sections. Scale bar = 100 μm. (E) The representative Western blotting bands of NLRP3 inflammasome and pyroptosis-associated proteins (ASC, NLRP3, Cle-Caps1, and GSDMD-NT) in mouse HL-1 cells under hypoxia treatments for different hours, n = 3 per group. (F) Quantification of the results of E, n = 3 per group. *p < 0.05, **p < 0.01, ***p < 0.001 relative to the sham or control group.

period in mice (Fig. 2B and C), and similar findings were also observed in the IHC staining (Fig. 2D). In the in vitro experiment, human AC-16 and mouse HL-1 cells were subjected to hypoxia for different periods (1 h, 3 h, and 6 h) to mimic the myocardial ischemia state in mice. Consistent with the results of the animal experiments, Western blotting analysis revealed a remarkable elevation in the levels of ASC, NLRP3, cleaved caspase-1, and GSDMD-NT in HL-1 (Fig. 2E and F) and AC-16 cells (Supplementary Figs. 1A and B) with prolonged hypoxia durations,

particularly prominent at the 6-h post-hypoxia (hypoxia-6h) time point. Collectively, these results strongly support that NLRP3 inflammasome-mediated cardiomyocyte pyroptosis is markedly activated and might be a major factor in AMI.

3.3. Inhibition of NLRP3 inflammasome-mediated pyroptosis reduced myocardial injury induced by hypoxia

To explore the potential impact of NLRP3 inflammasome and pyroptosis on myocardial injury resulting from hypoxia, we treated HL-1 cardiomyocytes with MCC950 (a selective NLRP3 inflammation inhibitor) and VX-765 (a specific caspase1 inhibitor). As illustrated in Fig. 3A and B, pharmacological inhibition of both NLRP3 inflammation and caspase1 effectively alleviated the expression levels of pyroptotic proteins under hypoxic condition. Meanwhile, treatment with MCC950 and VX-765 positively affected the survival of hypoxic cardiomyocytes, and neither of these treatments exhibited in vitro toxicity to mouse HL-1 myocytes (Fig. 3C) or human AC-16 myocytes (Supplementary Fig. 2) as determined by CCK-8 assay. Moreover, PI uptake was significantly increased in the hypoxia-6h group compared to the control group, while PI-positive cardiomyocytes were notably reduced in the groups co-treated with hypoxia and either MCC950 or VX-765 (Fig. 3D and E). These results suggested that the suppression of pyroptosis dependent on the NLRP3 inflammasome conferred protection against hypoxia-induced damage to cardiomyocytes.

3.4. Inactivation of NLRP3 inflammasome and pyroptosis blocked hypoxia-induced oxidative stress in vitro

To further understand the mechanisms underlying NLRP3

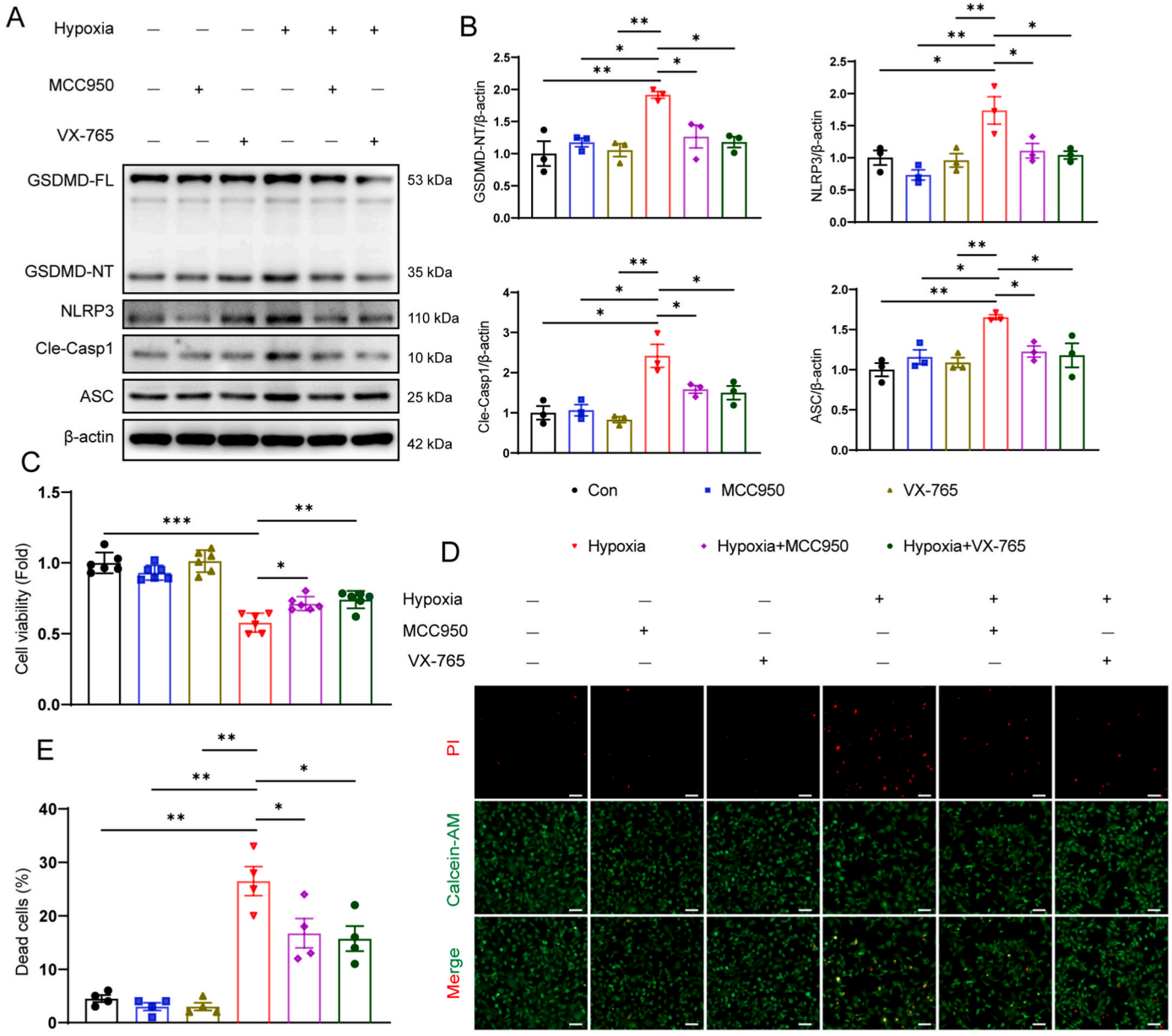

Fig. 3. Pharmacologic inhibitors of NLRP3 inflammasome and pyroptosis rescued hypoxia-induced cardiomyocytes injury. (A) The representative Western blotting bands of NLRP3 inflammasome and pyroptosis-associated proteins in cardiac HL-1 cells under indicated treatments. n = 3 per group. (B) Summary of western blotting results of A. n = 3 per group. (C) CCK-8 assay was performed to examine mouse HL-1 cells viability under indicated treatments. n = 6 per group. (D) Representative fluorescent staining images of Calcein-AM (green) and PI (red) in mouse HL-1 cells. Scale bar = 50 μm. (E) Summary of the Calcein/PI staining results of D, n = 4 per group. *p < 0.05, **p < 0.01, ***p < 0.001 as indicated.

inflammasome and pyroptosis-mediated cardiomyocytes damage under hypoxia condition, we initially assessed whether NLRP3 inflammasome-dependent pyroptosis influences the oxidative stress in cardiomyocytes subjected to hypoxia.

It is widely recognized that oxidative stress plays a significant role in AMI-induced cardiac injury and dysfunction [11,30,37]. Western blotting analysis revealed a substantial increase in the protein levels of the NADPH oxidase subunit 67phox (p67phox), an indicator of oxidative stress, in the hypoxia-6h group compared to the control group. However, this expression was rescued by treatment with either MCC950 or VX-765 in hypoxic cardiomyocytes (Fig. 4A and B). Furthermore, DCFH-DA staining demonstrated that specific pharmacological inhibitors of pyroptosis significantly attenuated ROS generation triggered by hypoxia (Fig. 4C and D). These data provided that inhibiting NLRP3 inflammasome-mediated pyroptosis mitigates oxidative stress damage caused by hypoxia in vitro.

3.5. Inactivation of NLRP3 inflammasome-dependent pyroptosis rescued hypoxia-induced apoptosis in myocytes

Cardiomyocytes apoptosis is a hallmark of AMI and exerts a pivotal influence on the pathological cascade of AMI [38,39], significantly contributing to myocyte death [40,41]. Consistently, hypoxia treatment remarkably increased the expression of apoptosis-realted markers BAX and cleaved Caspase3 (Cle-Caps3) while decreasing the expression of BCL2, which were abrogated in the presence of MCC950 or VX-765 (Fig. 5A and B). Moreover, TUNEL staining showed a marked rise in the incidence of apoptotic cardiomyocytes in response to hypoxia compared to the control group, the effect that was also blunted by MCC950 or VX-765 administration (Fig. 5C and D). These findings illustrated that inhibition of NLRP3 inflammasome-dependent pyroptosis could prevent cardiomyocytes apoptosis induced by hypoxia.

3.6. Inhibition of NLRP3 inflammasome-dependent pyroptosis alleviated hypoxia-induced inflammation in myocytes

In line with our transcriptome analysis, mounting evidence indicated that inflammation responses were activated following AMI, and excessive inflammatory factors can lead to the structural and functional abnormalities in the myocardium [42]. Compared with the control group, the levels of proinflammatory cytokines (TNF-α, IL-6, and MMP-9) were markedly elevated in hypoxia HL-1 cells, which was blunted by the incubation of MCC9650 or VX-765 (Fig. 6A and B). Notably, the phosphorylation of p65 was promoted by hypoxia insult, indicating its activation in cardiomyocytes. However, the administration of pyroptosis inhibitors significantly alleviated p65 activation in response to hypoxia (Fig. 6C and D). These data indicated that inhibition of pyroptosis alleviated hypoxia-induced inflammatory response, a process that may be associated with the activated NF-κB signaling pathway.

3.7. Circulating GSDMD significantly increased in both hypoxic cardiomyocytes in vitro and AMI mice in vivo

GSDMD, the pyroptosis executor, has been reported to be released by pyroptotic cardiomyocytes [27]. Therefore, we examined the changes in circulating GSDMD levels in blood and cell supernatants after AMI or hypoxia treatment to evaluate its diagnostic potential for AMI. GSDMD content was measured in mouse plasma at 1 h, 3 h, and 6 h after AMI using ELISA. As depicted in Fig. 7A, the concentration of plasma GSDMD gradually increased with the duration of infarction, peaking at 3 h after AMI. Intriguingly, we observed that as early as 1 h after AMI, the changes in GSDMD exhibited a significant elevation of 4–5 folds, which was notably higher compared to the increase (1.5–2 folds) observed in CK-MB (a classical biomarker for AMI diagnosis) (Fig. 7B). Additionally, a notable correlation ($r = 0.8353$, $p < 0.0001$) was observed between the changes in circulating GSDMD and CK-MB levels (Fig. 7C). Furthermore, we also noted that the levels of GSDMD in the supernatant of hypoxia cardiomyocytes increased depending on the duration of hypoxia in cardiac HL-1 cells (Fig. 7D) and AC-16 cells (Fig. 7E) as determined by ELISA and Western blotting. Collectively, these findings suggest that GSDMD holds the potential to emerge as a novel diagnostic biomarker for AMI.

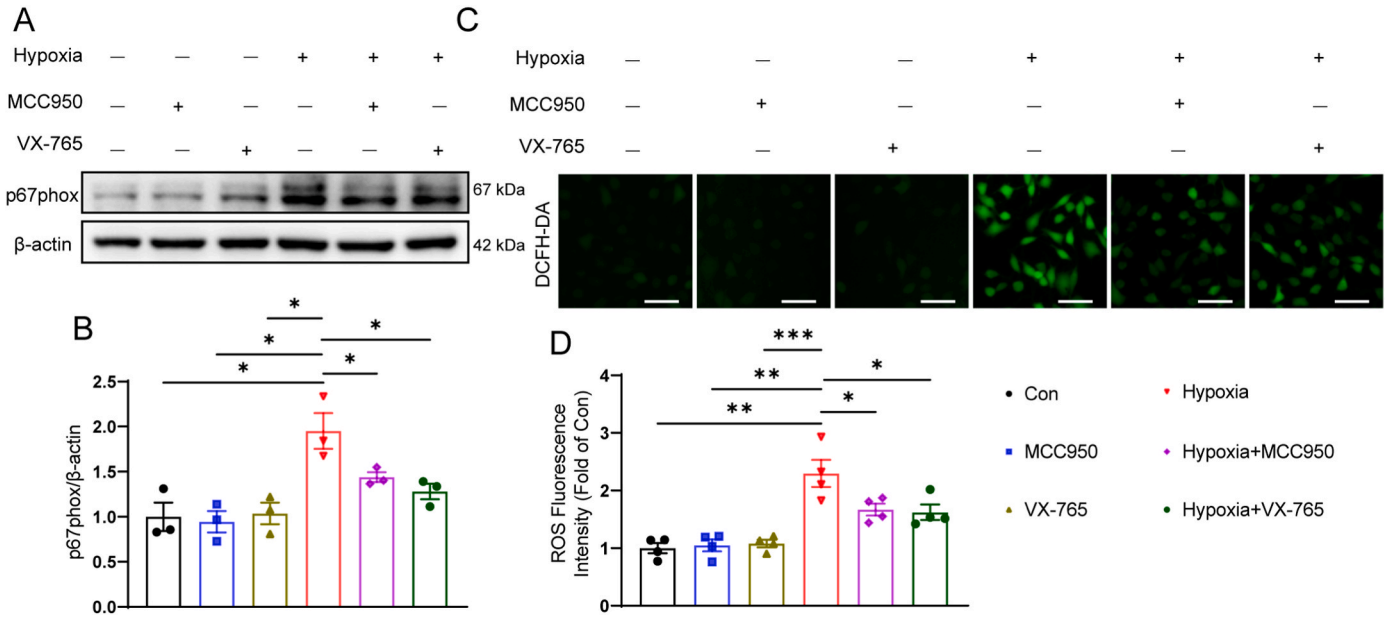

Fig. 4. Pharmacologic inhibitors of NLRP3 inflammasome and pyroptosis reduced hypoxia-induced oxidative stress in vitro. (A) The representative Western blotting bands of NADPH oxidase subunit 67phox (p67phox) in mouse HL-1 cells under indicated treatments. n = 3 per group. (B) Summary of western blotting results of A. n = 3 per group. (C) Representative images of DCFH-DA staining in mouse cardiac HL-1 cells under indicated treatments. Scale bar = 50 μm. (D) ROS levels were ascertained by quantifying DCFH-DA fluorescence. n = 4 per group. *p < 0.05, **p < 0.01, ***p < 0.001 as indicated.

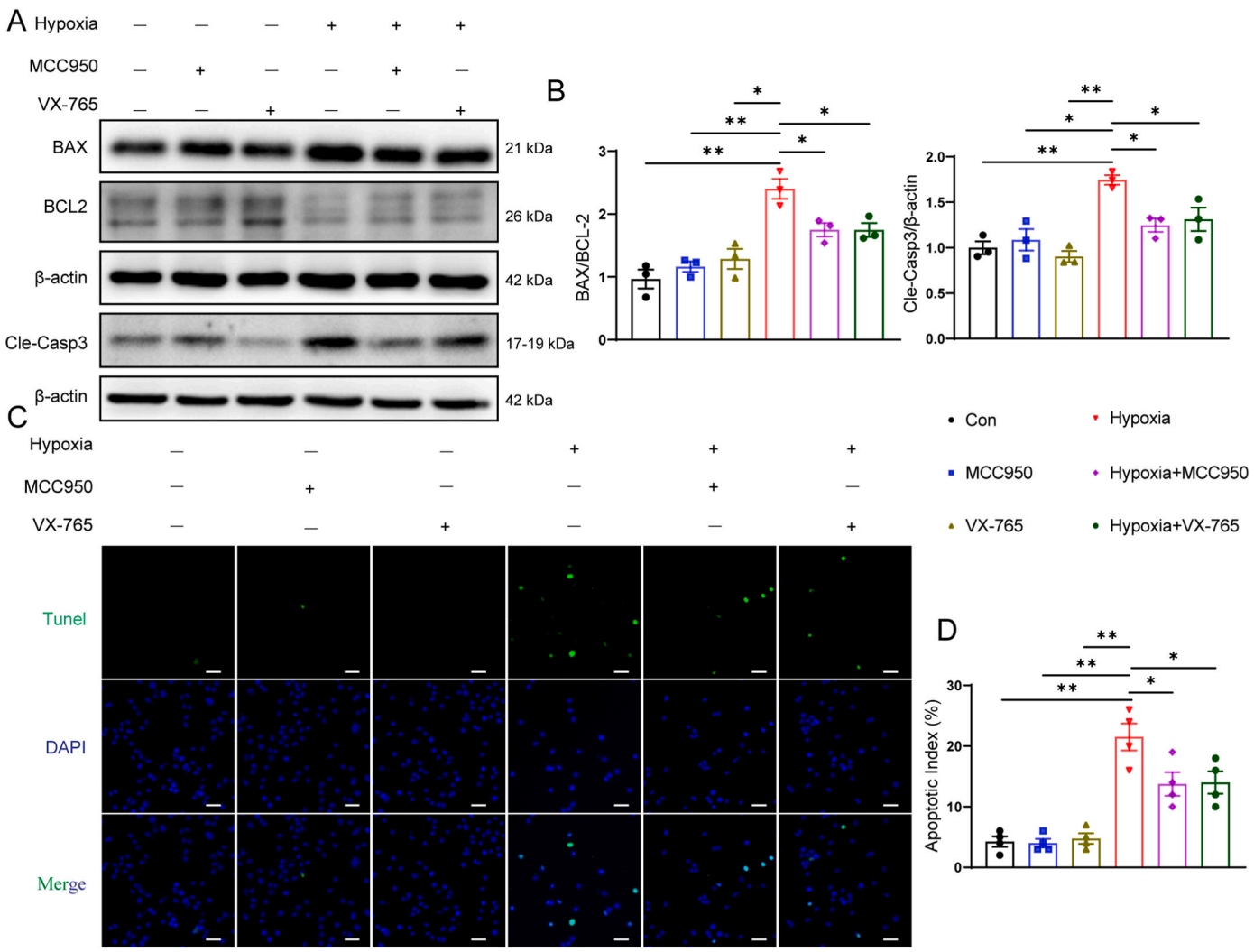

Fig. 5. Pharmacologic inhibition of NLRP3 inflammasome and pyroptosis reduced hypoxia-induced apoptosis in vitro. (A) The representative Western blotting bands of apoptosis-associated proteins (BAX, BCL2, and Cle-Casp3) in mouse HL-1 cells under indicated treatments. n = 3 per group. (B) Quantification of western blotting results of A. n = 3 per group. (C) Representative pictures of TUNEL staining in mouse cardiac HL-1 cells under indicated treatments. Green fluorescence indicates TUNEL-positive cell, blue fluorescence represents the nucleus of cardiomyocytes. Scale bar = 50 μm. n = 4 per group. (D) Quantification of apoptotic cardiomyocytes, which were presented as apoptotic index (× 100 %). *p < 0.05, **p < 0.01 as indicated.

4. Discussion

AMI is a severe cardiac condition with a high global mortality and morbidity rate. It can lead to serious cardiovascular incidents such as ventricular remodeling and heart failure, posing a significant risk to individuals' lives and resulting in substantial physical and financial burdens on patients [2,3]. Massive cardiomyocyte death is the predominant factor contributing to cardiac injury and impaired heart function resulting from AMI. Therefore, exploring the underlying molecular mechanisms of AMI-induced myocardial injury can yield valuable insights for the development of treatment strategies.

In this study, we initially successfully established an AMI mouse model, validated through ECG, echocardiography, CK-MB, and histological examinations. To elucidate the molecular alterations and biological processes during the early stages of AMI, we conducted RNA-seq analysis on infarcted myocardial tissues from both the AMI-3h and sham groups. Our transcriptome analysis identified 254 DEGs, with 226 up-regulated genes and 28 down-regulated genes. GO analysis revealed significant activation of processes related to inflammation response, such as leukocyte migration and leukocyte chemotaxis. Additionally, KEGG pathway analysis also showed enrichment of several inflammation-associated signaling pathways, including cytokine−cytokine receptor interaction, NOD−like receptor signaling pathway, IL-17 signaling pathway, TNF signaling pathway, NF−kappa B signaling pathway, and chemokine signaling pathway. These results indicated compelling evidence of the inflammatory process activation in the early phase of AMI, which is consistent with findings reported in other literature [9]. Pyroptosis, a form of programmed cell death, is closely associated with the inflammatory response [18]. Based on these findings, our subsequent research focused on investigating the relationship between pyroptosis and AMI. Our findings demonstrated significantly elevated expression levels of pyroptosis-associated proteins, including cleaved caspase1, NLRP3, GSDMD-NT, and ASC, in both a mouse model of AMI and a hypoxia-induced cell model in vitro. Similar results were obtained in human heart samples from autopsy cases of AMI. Therefore, these results suggest that AMI can trigger the induction of pyroptosis and may be a significant contributor to myocardial injury caused by AMI.

Pyroptosis, unlike traditional cell death such as apoptosis and necrosis, is primarily mediated by inflammasomes [20]. The NLRP3 inflammasome has been extensively acknowledged as a pivotal factor in triggering pyroptosis [43]. When external stimuli are detected by

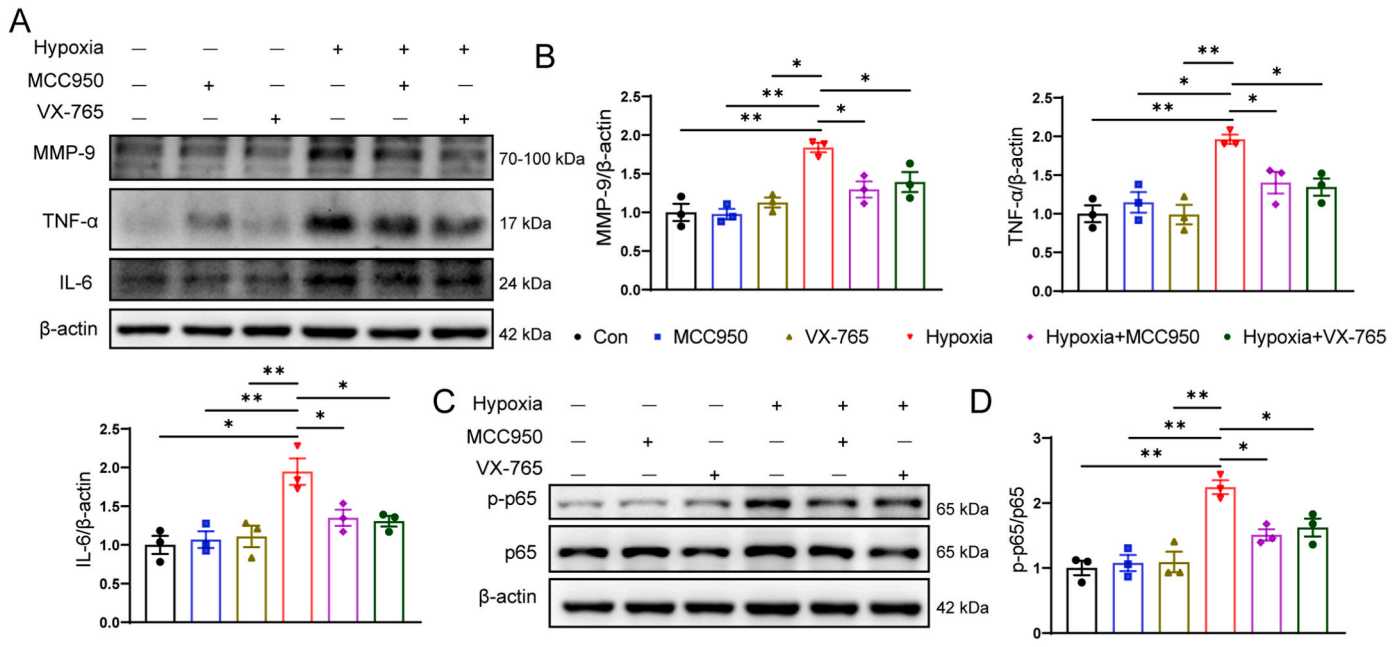

Fig. 6. Pharmacologic inhibition of NLRP3 inflammasome and pyroptosis suppressed hypoxia-induced inflammation in vitro. (A) The representative Western blotting bands of proinflammatory cytokines (IL-6, TNF-α, and MMP-9) in mouse HL-1 cells under indicated treatments. n = 3 per group. (B) Quantification of western blotting results of A. n = 3 per group. (C) The representative Western blotting bands of phosphorylation of p65 (p-p65) and p65 in mouse HL-1 cells under indicated treatments. n = 3 per group. (D) Summary of western blotting results of C. n = 3 per group. *p < 0.05, **p < 0.01 as indicated.

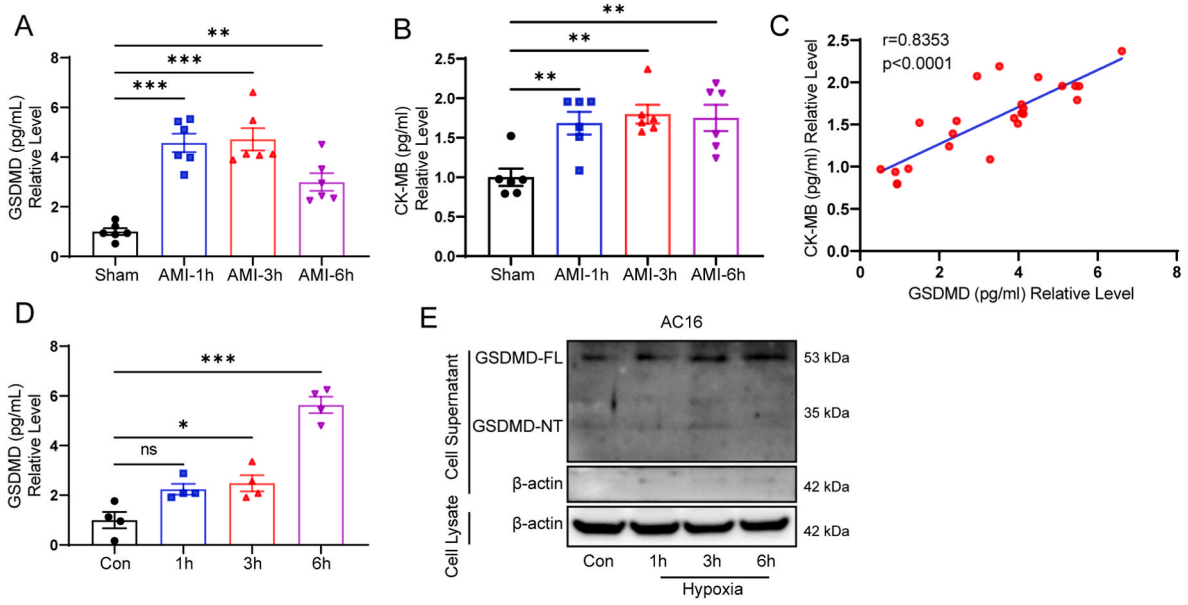

Fig. 7. Circulating GSDMD was significantly elevated in the plasma of mouse during the early infarction hours, as well as in the supernatant of hypoxic cardiac cells. (A) ELISA was performed to measure the circulating GSDMD in the plasma of mouse at different time points following AMI. n = 6 per group. (B) The levels of CK-MB were detected in the plasma of mouse at different time points following AMI by ELISA. (C) Linear correlation analysis was conducted between GSDMD and CK-MB levels in the plasma of sham group and AMI groups at 1 h, 3 h, and 6 h post-surgery (n = 6 per group, totaling 24 samples). (D) GSDMD levels were detected in the supernatants of cardiac HL-1 cells at different hypoxia times by ELISA. n = 4 per group. (E) The representative Western blotting bands of GSDMD in the culture supernatants of hypoxic AC-16 cells. *p < 0.05, **p < 0.01, ***p < 0.001 relative to the sham or control group.

pattern recognition receptors on the cell membrane and cytoplasm, NLRP3 is activated, recruiting ASC and caspase-1 for cleavage and ultimately leading to the formation of biologically active NLRP3 inflammasome [21]. Subsequently, the active caspase1 promotes the maturation and production of IL-1β and IL-18, while cleaving GSDMD to form GSDMD-NT. This process induces characteristic morphological changes such as cytoplasmic swelling and membrane rupture, ultimately resulting in cell death [21,22]. Our experiments consistently demonstrated that AMI induces the activation of NLRP3 inflammasome and triggers pyroptosis in cardiac myocytes. Meanwhile, pre-treatment with the selective NLRP3 inflammation inhibitor MCC950 and specific caspase1 suppressor inhibitor VX-765 not only significantly reduces hypoxia-induced cardiomyocyte death but also effectively suppresses inflammation, oxidative stress, and apoptosis resulting from hypoxia.

These findings suggested that inhibiting NLRP3 inflammasome-mediated pyroptosis can significantly alleviate myocardial damage caused by acute hypoxia, highlighting MCC950 and VX-765 as promising new strategies for the treatment of acute myocardial hypoxia or even AMI. Consistent with our study, Wenju et al. reported that VX-765 remarkably reduced cardiac damage and improved cardiac function in mice following AMI [44]. The combination of VX-765 and Ticagrelor, a P2Y12 antagonist, has been reported to attenuate AMI symptoms and sustain a reduction in infarct size in rats [45]. In a pig model of MI, the selective NLRP3 inflammasome inhibitor MCC950 has been also found to decrease infarct size and preserve cardiac function [46]. It is worth noting that small-molecule inhibitors targeting pyroptosis or the NLRP3 inflammasome have shown therapeutic potential in various disease models [47,48]. Moreover, a phase II clinical study has already been conducted to investigate the use of VX-765 for epilepsy treatment [49]. Therefore, our comprehensive investigation into the potential application of MCC950 and VX-765 in AMI treatment emphasizes the need for large-scale clinical trials to validate their therapeutic value.

Oxidative stress, inflammation and apoptosis are widely recognized as key contributors to the progression of AMI. Mounting evidence confirmed that oxidative stress-mediated cardiomyocyte apoptosis occurs in the early stages of AMI and is closely associated with adverse cardiovascular outcomes resulting from myocardial ischemia [12]. Mitochondria serve as the source of ROS, and excessive ROS accumulation induces mitochondrial damage, amplifying ROS levels and ultimately resulting in cell death [50]. So, maintaining mitochondrial equilibrium and decreasing ROS production is regarded as a potential approach to alleviate oxidative stress-induced damage. In the context of AMI, sustained hypoxia and mitochondrial dysfunction in cardiomyocytes lead to ATP deficiency, initiating apoptotic cascade activation and necrosis of myocardial cells. The necrotic cardiomyocytes activate the immune system, eliciting a robust inflammatory response [51]. Moreover, oxidative stress can intensify the inflammatory process by enhancing the expression of inflammatory cytokines and promoting leukocyte chemotaxis [13]. In this study, we observed a significant increase in oxidative stress, inflammation, and apoptotic cardiomyocytes in response to myocardial hypoxia. Remarkably, the administration of MCC950 and VX-765 notably mitigated these effects. These results suggested that the attenuation of myocardial injury resulting from inhibiting NLRP3 inflammasome-mediated pyroptosis may be associated with a reduction in oxidative stress, inflammation, and apoptosis. Further research is warranted to elucidate the molecular mechanisms underlying these observations, including the impact of mitochondrial dysfunction-induced oxidative stress on the pyroptosis process. Additionally, it is noteworthy that the phosphorylation of NF-κB p65 (p-p65) was induced by hypoxia, which was alleviated following pyroptosis inhibition. As commonly understood, the NF-κB signaling pathway is of paramount importance in mediating inflammatory processes. The up-regulation of inflammatory cytokines is attributed to the increase in ROS levels and the activation of p-p65 [52]. It has been observed that p65 facilitates the transcription of NLRP3 components, thereby influencing the release of downstream inflammatory mediators involved in the inflammatory response [53]. Based on these observations, we hypothesized that the treatment of MCC950 and VX-765 to suppress hypoxia-induced myocardial inflammation may involve modulation of the NF-κB signaling pathway.

Histological examination is considered as the gold standard for diagnosing many diseases. Regrettably, in the early stages of acute myocardial ischemia (within 4–6 h), the myocardial tissue does not exhibit diagnostically significant features due to the limited time available for the development of ischemic lesions, leading to the manifestation of non-specific findings, such as interstitial edema and wavy fibers, and hyper eosinophilia of cardiomyocytes [54,55]. Early diagnosis of AMI is crucial for patient treatment and prognosis. Therefore, the identification of specific and sensitive biomarkers for early detection of AMI holds considerable clinical significance. In this study, we discovered that GSDMD levels in the plasma of AMI mice increased gradually with the duration of ischemia, peaking at 3 h post-AMI. Notably, a significant 4–5 fold elevation in GSDMD levels was detected as early as 1 h post-AMI. Importantly, a significant correlation was found between the alterations in circulating GSDMD levels and CK-MB levels. In addition, we observed the release of GSDMD into the culture medium following hypoxia-induced myocardial pyroptosis in vitro. Collectively, these findings suggest that circulating GSDMD could serve as an early diagnostic biomarker for AMI. Therefore, we believe that combining GSDMD with conventional clinical diagnostic markers like cardiac troponins (cTnI and cTnT) and CK-MB may enhance the specificity of AMI diagnosis.

Nevertheless, we acknowledged the several limitations in our study. Firstly, we did not employ molecular techniques such as gene knockout or overexpression to manipulate key molecules involved in NLRP3 inflammasome-mediated pyroptosis to investigate their role in hypoxia or AMI. Secondly, the therapeutic effects of MCC950 and VX-765 in hypoxia still require further investigation in animal models of AMI. Additionally, the feasibility of utilizing circulating GSDMD as a diagnostic marker for AMI requires validation through clinical trials for practical application. In the future, it would be important and urgent to further investigate the molecular mechanisms underlying myocardial pyroptosis-induced AMI damage through in vitro and in vivo experiments.

5. Conclusion

In conclusion, our results suggested that NLRP3 inflammasome-mediated pyroptosis is a key contributor to the pathological process of AMI, which involves oxidative stress, inflammation, and myocardial apoptosis induced by acute myocardial hypoxia. The administration of MCC950 and VX-765 may represent novel therapeutic approaches for AMI treatment. Further, the circulating GSDMD exhibits potential as an early diagnostic biomarker for AMI.

Funding

This work was supported by the Key Projects of National Natural Science Foundation of China (Grant Number.: 81430047), and National Key Research and Development Program (Grant Number.: 2018 YFC0807202).

CRediT authorship contribution statement

Xing Ye: Writing – original draft, Visualization, Methodology, Investigation, Formal analysis, Conceptualization. **Zi-jie Lin:** Validation, Methodology, Investigation, Formal analysis, Data curation. **Guang-hui Hong:** Validation, Formal analysis, Data curation. **Zhi-min Wang:** Validation, Supervision, Investigation, Data curation. **Run-ting Dou:** Validation, Supervision, Investigation, Data curation. **Jun-yi Lin:** Writing – review & editing, Supervision, Conceptualization. **Jian-hui Xie:** Writing – review & editing, Supervision, Project administration, Funding acquisition, Conceptualization. **Yi-wen Shen:** Writing – review & editing, Supervision, Project administration, Funding acquisition, Conceptualization.

Declaration of competing interest

All authors declare no competing interest.

Data availability

Data will be made available on request.

Appendix A. Supplementary data

Supplementary data to this article can be found online at https://doi.org/10.1016/j.yexcr.2024.114061.

References

[1] J.L. Anderson, D.A. Morrow, Acute myocardial infarction, N. Engl. J. Med. 376 (2017) 2053–2064.
[2] Y. Zhang, L. Jiao, L. Sun, Y. Li, Y. Gao, C. Xu, Y. Shao, M. Li, C. Li, Y. Lu, Z. Pan, L. Xuan, Y. Zhang, Q. Li, R. Yang, Y. Zhuang, Y. Zhang, B. Yang, LncRNA ZFAS1 as a SERCA2a inhibitor to cause intracellular Ca(2+) Overload and contractile dysfunction in a mouse model of myocardial infarction, Circ. Res. 122 (2018) 1354–1368.
[3] Y. Lu, Y. Zhang, H. Shan, Z. Pan, X. Li, B. Li, C. Xu, B. Zhang, F. Zhang, D. Dong, W. Song, G. Qiao, B. Yang, MicroRNA-1 downregulation by propranolol in a rat model of myocardial infarction: a new mechanism for ischaemic cardioprotection, Cardiovasc. Res. 84 (2009) 434–441.
[4] D. Jenca, V. Melenovsky, J. Stehlik, V. Stanek, J. Kettner, J. Kautzner, V. Adamkova, P. Wohlfahrt, Heart failure after myocardial infarction: incidence and predictors, ESC Heart Fail 8 (2021) 222–237.
[5] F.S. Apple, Y. Sandoval, A.S. Jaffe, J. Ordonez-Llanos, I.T.F.o.C.A.o.C. Bio-Markers, Cardiac troponin assays: guide to understanding analytical characteristics and their impact on clinical care, Clin. Chem. 63 (2017) 73–81.
[6] S. Aydin, K. Ugur, S. Aydin, I. Sahin, M. Yardim, Biomarkers in acute myocardial infarction: current perspectives, Vasc. Health Risk Manag. 15 (2019) 1–10.
[7] M. Rubini Gimenez, R. Twerenbold, T. Reichlin, K. Wildi, P. Haaf, M. Schaefer, C. Zellweger, B. Moehring, F. Stallone, S.M. Sou, M. Mueller, K. Denhaerynck, T. Mosimann, M. Reiter, B. Meller, M. Freese, C. Stelzig, I. Klimmeck, J. Voegele, B. Hartmann, K. Rentsch, S. Osswald, C. Mueller, Direct comparison of high-sensitivity-cardiac troponin I vs. T for the early diagnosis of acute myocardial infarction, Eur. Heart J. 35 (2014) 2303–2311.
[8] B.L. Zhu, T. Ishikawa, T. Michiue, D.R. Li, D. Zhao, Y. Bessho, Y. Kamikodai, K. Tsuda, S. Okazaki, H. Maeda, Postmortem cardiac troponin I and creatine kinase MB levels in the blood and pericardial fluid as markers of myocardial damage in medicolegal autopsy, Leg. Med. 9 (2007) 241–250.
[9] N.G. Frangogiannis, Regulation of the inflammatory response in cardiac repair, Circ. Res. 110 (2012) 159–173.
[10] C. Zhai, G. Qian, H. Wu, H. Pan, S. Xie, Z. Sun, P. Shao, G. Tang, H. Hu, S. Zhang, Knockdown of circ_0060745 alleviates acute myocardial infarction by suppressing NF-kappaB activation, J. Cell Mol. Med. 24 (2020) 12401–12410.
[11] B. Liang, X.X. Zhang, R. Li, Y.C. Zhu, X.J. Tian, N. Gu, Guanxin V alleviates acute myocardial infarction by restraining oxidative stress damage, apoptosis, and fibrosis through the TGF-beta1 signalling pathway, Phytomedicine 100 (2022) 154077.
[12] M. Tomandlova, J. Parenica, P. Lokaj, T. Ondrus, P. Kala, M. Miklikova, K. Helanova, M. Helan, J. Malaska, K. Benesova, J. Jarkovsky, M. Pavkova Goldbergova, J. Tomandl, Prognostic value of oxidative stress in patients with acute myocardial infarction complicated by cardiogenic shock: a prospective cohort study, Free Radic. Biol. Med. 174 (2021) 66–72.
[13] C.E. Murdoch, S. Chaubey, L. Zeng, B. Yu, A. Ivetic, S.J. Walker, D. Vanhoutte, S. Heymans, D.J. Grieve, A.C. Cave, A.C. Brewer, M. Zhang, A.M. Shah, Endothelial NADPH oxidase-2 promotes interstitial cardiac fibrosis and diastolic dysfunction through proinflammatory effects and endothelial-mesenchymal transition, J. Am. Coll. Cardiol. 63 (2014) 2734–2741.
[14] D. Yao, B. Shi, S. Wang, L. Bao, M. Tan, H. Shen, Z. Zhang, X. Pan, Y. Yang, Y. Wu, K. Gong, Isoliquiritigenin ameliorates ischemia-induced myocardial injury via modulating the Nrf2/HO-1 pathway in mice, Drug Des Devel Ther 16 (2022) 1273–1287.
[15] H.D. White, K. Thygesen, J.S. Alpert, A.S. Jaffe, Clinical implications of the third universal definition of myocardial infarction, Heart 100 (2014) 424–432.
[16] M.F. Minicucci, P.S. Azevedo, B.F. Polegato, S.A. Paiva, L.A. Zornoff, Heart failure after myocardial infarction: clinical implications and treatment, Clin. Cardiol. 34 (2011) 410–414.
[17] R.S. Whelan, V. Kaplinskiy, R.N. Kitsis, Cell death in the pathogenesis of heart disease: mechanisms and significance, Annu. Rev. Physiol. 72 (2010) 19–44.
[18] A. Zychlinsky, M.C. Prevost, P.J. Sansonetti, Shigella flexneri induces apoptosis in infected macrophages, Nature 358 (1992) 167–169.
[19] B. Kolbrink, T. Riebeling, U. Kunzendorf, S. Krautwald, Plasma membrane pores drive inflammatory cell death, Front. Cell Dev. Biol. 8 (2020) 817.
[20] S. Toldo, A. Abbate, The role of the NLRP3 inflammasome and pyroptosis in cardiovascular diseases, Nat. Rev. Cardiol. 21 (2023) 219–237.
[21] S.M. Man, R. Karki, T.D. Kanneganti, Molecular mechanisms and functions of pyroptosis, inflammatory caspases and inflammasomes in infectious diseases, Immunol. Rev. 277 (2017) 61–75.
[22] W.T. He, H. Wan, L. Hu, P. Chen, X. Wang, Z. Huang, Z.H. Yang, C.Q. Zhong, J. Han, Gasdermin D is an executor of pyroptosis and required for interleukin-1beta secretion, Cell Res. 25 (2015) 1285–1298.
[23] Y. Zhang, X. Liu, X. Bai, Y. Lin, Z. Li, J. Fu, M. Li, T. Zhao, H. Yang, R. Xu, J. Li, J. Ju, B. Cai, C. Xu, B. Yang, Melatonin prevents endothelial cell pyroptosis via regulation of long noncoding RNA MEG3/miR-223/NLRP3 axis, J. Pineal Res. 64 (2018) e12449.
[24] I. Jorgensen, E.A. Miao, Pyroptotic cell death defends against intracellular pathogens, Immunol. Rev. 265 (2015) 130–142.
[25] X. Li, N. Du, Q. Zhang, J. Li, X. Chen, X. Liu, Y. Hu, W. Qin, N. Shen, C. Xu, Z. Fang, Y. Wei, R. Wang, Z. Du, Y. Zhang, Y. Lu, MicroRNA-30d regulates cardiomyocyte pyroptosis by directly targeting foxo3a in diabetic cardiomyopathy, Cell Death Dis. 5 (2014) e1479.
[26] N.G. Frangogiannis, The inflammatory response in myocardial injury, repair, and remodelling, Nat. Rev. Cardiol. 11 (2014) 255–265.
[27] H. Shi, Y. Gao, Z. Dong, J. Yang, R. Gao, X. Li, S. Zhang, L. Ma, X. Sun, Z. Wang, F. Zhang, K. Hu, A. Sun, J. Ge, GSDMD-mediated cardiomyocyte pyroptosis promotes myocardial I/R injury, Circ. Res. 129 (2021) 383–396.
[28] E. Gao, Y.H. Lei, X. Shang, Z.M. Huang, L. Zuo, M. Boucher, Q. Fan, J.K. Chuprun, X.L. Ma, W.J. Koch, A novel and efficient model of coronary artery ligation and myocardial infarction in the mouse, Circ. Res. 107 (2010) 1445–1453.
[29] X. Ye, J. Lin, Z. Lin, A. Xue, L. Li, Z. Zhao, L. Liu, Y. Shen, B. Cong, Axin1 up-regulated 1 accelerates stress-induced cardiomyocytes apoptosis through activating Wnt/beta-catenin signaling, Exp. Cell Res. 359 (2017) 441–448.
[30] L. Mei, Y. Chen, P. Chen, H. Chen, S. He, C. Jin, Y. Wang, Z. Hu, W. Li, L. Jin, W. Cong, X. Wang, X. Guan, Fibroblast growth factor 7 alleviates myocardial infarction by improving oxidative stress via PI3Kalpha/AKT-mediated regulation of Nrf2 and HXK2, Redox Biol. 56 (2022) 102468.
[31] Y. Feng, W. Huang, W. Meng, A.G. Jegga, Y. Wang, W. Cai, H.W. Kim, Z. Pasha, Z. Wen, F. Rao, R.M. Modi, X. Yu, M. Ashraf, Heat shock improves Sca-1+ stem cell survival and directs ischemic cardiomyocytes toward a prosurvival phenotype via exosomal transfer: a critical role for HSF1/miR-34a/HSP70 pathway, Stem Cell. 32 (2014) 462–472.
[32] L. Li, P. Gao, X. Tang, Z. Liu, M. Cao, R. Luo, X. Li, J. Wang, X. Lin, C. Peng, Z. Li, J. Zhang, X. Zhang, Z. Cao, Y. Zou, L. Jin, CB1R-stabilized NLRP3 inflammasome drives antipsychotics cardiotoxicity, Signal Transduct Target Ther 7 (2022) 190.
[33] X. Lin, Z. Lin, X. Zhao, Z. Liu, C. Xu, B. Yu, P. Gao, Z. Wang, J. Ge, Y. Shen, L. Li, Serum SELENBP1 and VCL are effective biomarkers for clinical and forensic diagnosis of coronary artery spasm, Int. J. Mol. Sci. 23 (2022) 13266.
[34] D.R. Green, The coming decade of cell death research: five riddles, Cell 177 (2019) 1094–1107.
[35] S. Toldo, A. Abbate, The NLRP3 inflammasome in acute myocardial infarction, Nat. Rev. Cardiol. 15 (2018) 203–214.
[36] S. Toldo, E. Mezzaroma, L.F. Buckley, N. Potere, M. Di Nisio, G. Biondi-Zoccai, B. W. Van Tassell, A. Abbate, Targeting the NLRP3 inflammasome in cardiovascular diseases, Pharmacol. Ther. 236 (2022) 108053.
[37] L. Hou, J. Guo, F. Xu, X. Weng, W. Yue, J. Ge, Cardiomyocyte dimethylarginine dimethylaminohydrolase1 attenuates left-ventricular remodeling after acute myocardial infarction: involvement in oxidative stress and apoptosis, Basic Res. Cardiol. 113 (2018) 28.
[38] J.W. Thompson, R.M. Graham, K.A. Webster, DNase activation by hypoxia-acidosis parallels but is independent of programmed cell death, Life Sci. 91 (2012) 223–229.
[39] S. Jia, X. Qiao, J. Ye, X. Fang, C. Xu, Y. Cao, M. Zheng, Nogo-C regulates cardiomyocyte apoptosis during mouse myocardial infarction, Cell Death Dis. 7 (2016) e2432.
[40] B.J. Han, G.Y. Cao, L.Y. Jia, G. Zheng, L. Zhang, P. Sheng, J.Z. Xie, C.F. Zhang, Cardioprotective effects of tetrahydropalmatine on acute myocardial infarction in rats, Am. J. Chin. Med. 50 (2022) 1887–1904.
[41] A. Abbate, R. Bussani, M.S. Amin, G.W. Vetrovec, A. Baldi, Acute myocardial infarction and heart failure: role of apoptosis, Int. J. Biochem. Cell Biol. 38 (2006) 1834–1840.
[42] J.T. Thackeray, H.C. Hupe, Y. Wang, J.P. Bankstahl, G. Berding, T.L. Ross, J. Bauersachs, K.C. Wollert, F.M. Bengel, Myocardial inflammation predicts remodeling and neuroinflammation after myocardial infarction, J. Am. Coll. Cardiol. 71 (2018) 263–275.
[43] I. Scholwer, P. Habib, C. Voelz, L. Rolfes, C. Beyer, A. Slowik, NLRP3 depletion fails to mitigate inflammation but restores diminished phagocytosis in BV-2 cells after in vitro hypoxia, Mol. Neurobiol. 57 (2020) 2588–2599.
[44] W. Liu, J. Shen, Y. Li, J. Wu, X. Luo, Y. Yu, Y. Zhang, L. Gu, X. Zhang, C. Jiang, J. Li, Pyroptosis inhibition improves the symptom of acute myocardial infarction, Cell Death Dis. 12 (2021) 852.
[45] J.P. Audia, X.M. Yang, E.S. Crockett, N. Housley, E.U. Haq, K. O'Donnell, M. V. Cohen, J.M. Downey, D.F. Alvarez, Caspase-1 inhibition by VX-765 administered at reperfusion in P2Y(12) receptor antagonist-treated rats provides long-term reduction in myocardial infarct size and preservation of ventricular function, Basic Res. Cardiol. 113 (2018) 32.
[46] G.P. van Hout, L. Bosch, G.H. Ellenbroek, J.J. de Haan, W.W. van Solinge, M. A. Cooper, F. Arslan, S.C. de Jager, A.A. Robertson, G. Pasterkamp, I.E. Hoefer, The selective NLRP3-inflammasome inhibitor MCC950 reduces infarct size and preserves cardiac function in a pig model of myocardial infarction, Eur. Heart J. 38 (2017) 828–836.
[47] B. Das, C. Sarkar, V.S. Rawat, D. Kalita, S. Deka, A. Agnihotri, Promise of the NLRP3 inflammasome inhibitors in in vivo disease models, Molecules 26 (2021) 4996.
[48] X. Zhang, Z. Wang, Y. Zheng, Q. Yu, M. Zeng, L. Bai, L. Yang, M. Guo, X. Jiang, J. Gan, Inhibitors of the NLRP3 inflammasome pathway as promising therapeutic candidates for inflammatory diseases (Review), Int. J. Mol. Med. 51 (2023) 35.
[49] I. Younus, D.S. Reddy, A resurging boom in new drugs for epilepsy and brain disorders, Expert Rev Clin Pharmacol 11 (2018) 27–45.
[50] S.J. Dixon, B.R. Stockwell, The role of iron and reactive oxygen species in cell death, Nat. Chem. Biol. 10 (2014) 9–17.
[51] S. Khodayari, H. Khodayari, A.Z. Amiri, M. Eslami, D. Farhud, J. Hescheler, K. Nayernia, Inflammatory microenvironment of acute myocardial infarction

prevents regeneration of heart with stem cells therapy, Cell. Physiol. Biochem. 53 (2019) 887–909.
[52] V. Blas-Valdivia, D.N. Moran-Dorantes, P. Rojas-Franco, M. Franco-Colin, N. Mirhosseini, R. Davarnejad, A. Halajisani, O. Tavakoli, E. Cano-Europa, C-Phycocyanin prevents acute myocardial infarction-induced oxidative stress, inflammation and cardiac damage, Pharm. Biol. 60 (2022) 755–763.
[53] L. Luo, M. Liu, Y. Fan, J. Zhang, L. Liu, Y. Li, Q. Zhang, H. Xie, C. Jiang, J. Wu, X. Xiao, Y. Wu, Intermittent theta-burst stimulation improves motor function by inhibiting neuronal pyroptosis and regulating microglial polarization via TLR4/NFkappaB/NLRP3 signaling pathway in cerebral ischemic mice, J. Neuroinflammation 19 (2022) 141.
[54] C. Ortmann, H. Pfeiffer, B. Brinkmann, A comparative study on the immunohistochemical detection of early myocardial damage, Int J Legal Med 113 (2000) 215–220.
[55] S.D. Visona, D. Benati, M.C. Monti, M. Galie, L. Andrello, A. Frontini, A. Osculati, Diagnosis of sudden cardiac death due to early myocardial ischemia: an ultrastructural and immunohistochemical study, Eur. J. Histochem. 62 (2018) 2866.

Abbreviations

AMI: acute myocardial infarction
FC: fold change
EF: ejection fraction
Not sig: not significant
Con: control
CK-MB: creatine Kinase-MB
GSDMD-NT: N-terminal of gasdermin D
GSDMD-FL: full-length of gasdermin D
Cle-Casp1: cleaved Caspase1
Cle-Casp3: cleaved Caspase3
GO: Gene Ontology
KEGG: Kyoto Encyclopedia of Genes and Genomes